

Broadband Axion Dark Matter Haloscopes via Electric Field Sensing

Ben T. McAllister,^{1,*} Maxim Goryachev,¹ Jeremy Bourhill,¹ Eugene N. Ivanov,¹ and Michael E. Tobar^{1,†}

¹*ARC Centre of Excellence For Engineered Quantum Systems,
Department of Physics, School of Physics and Mathematics,
University of Western Australia, 35 Stirling Highway, Crawley WA 6009, Australia.*
(Dated: May 18, 2022)

The mass of axion dark matter is only weakly bounded by cosmological observations, necessitating a variety of detection techniques in many different mass ranges. Axions are expected to convert to photons via the inverse Primakoff effect and cryogenic resonant cavities are often proposed as tools for detecting these photons. However, such structures are inherently narrowband and the range of possible axion dark matter masses spans several orders of magnitude. On the other hand broadband low-mass detectors have been proposed using inductive magnetometer sensors and a gapped toroidal solenoid magnet. In this work we propose an alternative, which uses a capacitive sensor in a conventional solenoidal magnet aligned in the laboratory z-axis, as implemented in standard haloscope experiments. In the presence of the DC magnetic field, the inverse Primakoff effect causes a time varying electric field (or displacement current) in the z-direction to oscillate at the axion Compton frequency. We propose non-resonant techniques to detect this electric field by implementing capacitive sensors coupled to a low noise amplifier. We present the theoretical foundation for this proposal, and the first experimental results. Preliminary results constrain $g_{a\gamma\gamma} > \sim 2.35 \times 10^{-12} \text{ GeV}^{-1}$ in the mass range of 2.08×10^{-11} to $2.2 \times 10^{-11} \text{ eV}$, and demonstrate potential sensitivity to axion-like dark matter with masses in the range of 10^{-12} to 10^{-8} eV .

For decades numerous cosmological observations have suggested the presence of a large amount of excess matter in the universe of unknown composition [1, 2]. The lack of direct observation suggests the matter is only very weakly interacting with standard model particles - it is known as “dark” matter. Many types of new particles have been proposed to account for the dark matter, over a vast mass range (sub-eV to GeV). Consequently we need a large number of experiments at various mass scales. Recent cosmological evidence combined with the null results of many experiments points away from the traditional WIMP hypotheses, and towards the low-mass regime [3–5]. This work focuses on low mass axions or axion like particles (ALPs), which are hypothetical neutral, spin zero bosons often proposed to solve the strong charge-parity problem in QCD[6–8]. Axions and ALPs can be formulated as dark matter [9], and if this is true they should be abundant in the laboratory frame on earth, and thus detectable. The most often explored ALP to standard model coupling is via the inverse Primakoff effect. In this coupling an axion interacts with a photon (usually a virtual photon supplied by a DC magnetic field) and converts into a second real photon such that;

$$\hbar\omega_a \approx m_a c^2 + \frac{1}{2}m_a v_a^2,$$

where m_a is the mass of the axion, ω_a is the frequency of the generated real photon, \hbar is the reduced Planck’s constant, c is the speed of light, and v_a is the velocity of the axion with respect to the laboratory frame, the distribution of axion velocities with respect to earth gives a “line-width” or effective quality-factor for the axion signal of approximately 10^6 [10, 11].

The strength of this axion-photon interaction, and the

mass of the axion are given by,

$$g_{a\gamma\gamma} = \frac{g_\gamma \alpha}{f_a \pi}, \quad m_a = \frac{z^{1/2}}{1+z} \frac{f_\pi m_\pi}{f_a}.$$

Here z is the ratio of up and down quark masses, $\frac{m_u}{m_d} \approx 0.56$, f_π is the pion decay constant $\approx 93 \text{ MeV}$, m_π is the neutral pion mass $\approx 135 \text{ MeV}$, g_γ is an axion-model dependent parameter of order 1, and α is the fine structure constant [12–16]. Confounding experimental efforts to detect axions via this coupling is the fact that f_a , the Peccei-Quinn Symmetry Breaking Scale, is unknown, and hence both the mass and strength of axion-photon coupling are unknown. This means that the photon frequency and amplitude of any axion induced signals are unknown, although we do have some broad limits from cosmological observations and previous experiments [17, 18]. There are theoretical predictions for axions over a wide range of masses, and a host of experiments and proposals exploring these mass ranges [19–29]. Most experiments that exploit the Primakoff effect rely on a tunable resonant structure designed to detect photons generated by axion conversion. The specific design depends heavily on the axion mass range, but most dark matter axion detection experiments operate in the microwave and millimeter-wave regimes. These experiments are inherently narrowband, which is a limitation, as the axion mass and therefore the corresponding photon frequency is unknown.

More recently ABRACADABRA was proposed, which is partly a broadband low-mass particle haloscope [26] designed to detect the photons generated by low mass, pre-inflationary dark matter axions. This experiment uses a solenoid magnet of gapped toroidal geometry and via the inverse Primakoff effect produces an oscillating mag-

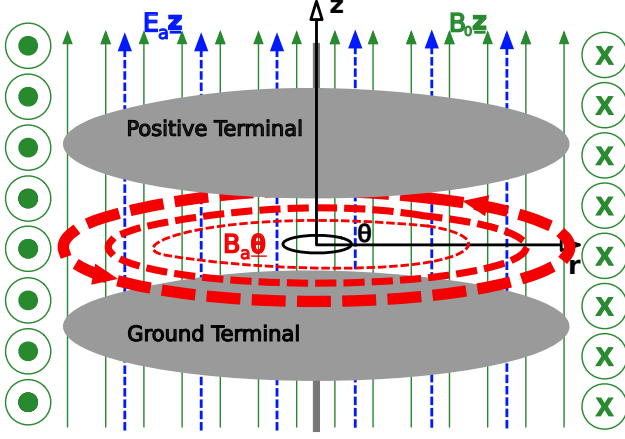


FIG. 1: A sketch of the proposed experiment, showing the static magnetic field (green) and the axion-induced fields (blue and red), along with the alignment of the capacitor.

netic field at the Compton frequency in the laboratory z -direction. The oscillating magnetic field is detected by an inductive magnetometer sensor coil coupled to a SQUID amplifier. In contrast, we propose a technique that may be implemented in the same setup as a standard resonant haloscope with a conventional solenoidal DC magnetic field aligned in the z -direction. It is well known in this setup that the inverse Primakoff effect induces a time varying electric field (which may be interpreted as a displacement current) aligned with the DC magnetic field oscillating at the axion Compton frequency. We propose non-resonant techniques to detect this electric field by considering capacitive sensors coupled to low noise current and voltage amplifiers. We name this experiment: **B**roadband **E**lectric-field **A**xion **S**ensing **T**echnique, or **BEAST**.

In order to derive the axion-modified Maxwell's equations, we begin with the Lagrangian for axions coupled to photons

$$\mathcal{L} = \frac{1}{2}(\partial_\mu a)^2 - \frac{1}{2}m_a^2 a^2 - \frac{1}{4}F_{\mu\nu}F^{\mu\nu} + \frac{1}{4}g_{a\gamma\gamma}aF_{\mu\nu}\tilde{F}^{\mu\nu}.$$

From this it can be shown that we arrive at the modified Maxwell's equations (in SI units, in media) [30],

$$\begin{aligned} \epsilon_r \vec{\nabla} \cdot \vec{E} &= \frac{\rho}{\epsilon_0} + g_{a\gamma\gamma} c \vec{B} \cdot \nabla a, \\ \frac{1}{\mu_r} \vec{\nabla} \times \vec{B} - \frac{1}{c^2} \epsilon_r \frac{\partial \vec{E}}{\partial t} &= \mu_0 \vec{J} - \frac{g_{a\gamma\gamma}}{c} \left(\vec{B} \frac{\partial a}{\partial t} + \nabla a \times \vec{E} \right), \\ \vec{\nabla} \cdot \vec{B} &= 0, \\ \vec{\nabla} \times \vec{E} &= -\frac{\partial \vec{B}}{\partial t}. \end{aligned}$$

Here \vec{E} is electric field, ρ is charge density, ϵ_r and ϵ_0 are

the relative and vacuum permittivity, \vec{B} is magnetic field, a is the axion scalar field, μ_r and μ_0 are the relative and vacuum permeability, c is the speed of light in vacuum, and \vec{J} is current density. Note that all terms containing $g_{a\gamma\gamma}$ are often presented with the opposite sign, but it has no impact on this work. With these relationships we can find the RF photonic fields induced by axion conversion in the cylindrical solenoidal magnetic field ($\vec{B} = B_0 \hat{z}$). These are given by [31] (see appendix for more detail),

$$\begin{aligned} \vec{E}_a &= E_a \hat{z} = \frac{1}{\epsilon_r} g_{a\gamma\gamma} c B_0 a \hat{z}, \\ \vec{B}_a &= \mu_r \frac{1}{2} \frac{g_{a\gamma\gamma}}{c} r B_0 \frac{\partial a}{\partial t} \hat{\phi}. \end{aligned}$$

Here r is the distance from the centre of the solenoid, and \hat{z} and $\hat{\phi}$ are the z -direction and ϕ -direction unit vectors in the cylindrical co-ordinate system of the solenoid.

Now we consider the detection of the electric field produced by the inverse Primakoff effect by monitoring the signal from a parallel plate capacitor embedded in the magnetic field, such that the vector area of the plates are aligned with the induced electric field. From the RF fields the expected voltage and current output from such a capacitor due to Primakoff axion conversion can be derived. The capacitance of a parallel plate capacitor with plate area A and separation d is given by $C = \frac{\epsilon_0 \epsilon_r A}{d}$. The voltage across the plates as a result of the axion induced electric field, \vec{E}_a is given by

$$V = \int_0^d E_a dz = \frac{1}{\epsilon_r} g_{a\gamma\gamma} c B_0 a d,$$

where $a = a_0 \cos(\omega_a t)$ and $a_0 = \sqrt{\frac{2\rho_a}{c} \frac{\hbar}{m_a}}$ [32]. We can now derive (see appendix),

$$\begin{aligned} I_{a_{RMS}} &= -g_{a\gamma\gamma} \epsilon_0 A B_0 \sqrt{\rho_a c^5} \\ V_{a_{RMS}} &= \frac{1}{\epsilon_r} g_{a\gamma\gamma} B_0 \sqrt{\rho_a c^5} \frac{1}{\omega_a} d. \end{aligned} \quad (1)$$

Interestingly, neither the capacitor plate separation nor the permittivity between the plates has an impact on the expected current, however, the area of the capacitor plates is an important factor. Conversely, the voltage across the plates depends only on the permittivity and the plate separation, not the area. An optimal detector for such an experiment thus depends on the method of readout. If we wish to read current with, for example a SQUID, we would implement the largest diameter capacitors that would fit inside the magnet bore. If we were to read voltage directly with, for example, a high-impedance amplifier, we would design for the lowest permittivity and largest plate separation achievable. However, one must be mindful that the derivation assumes an ideal parallel plate structure, with no fringing or parasitic capacitance.

The axion source term in the modified Maxwell's equations can be represented as an effective current density

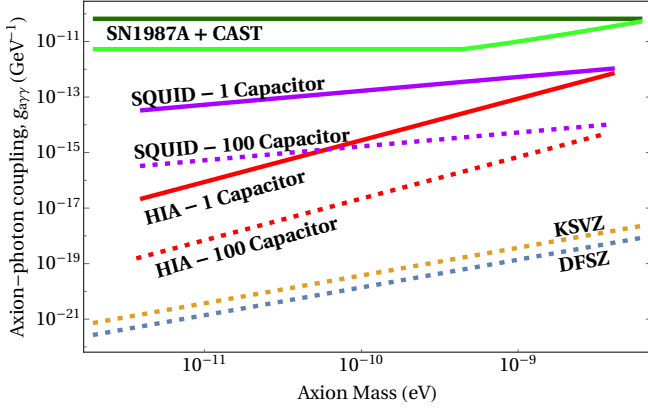


FIG. 2: Projected limits for the BEAST experiment, utilizing: a single capacitor (purple) and 100 capacitors (purple, dashed) coupled to a SQUID, and a single capacitor (red) and 100 capacitors (red, dashed) coupled to a high-impedance amplifier. Current best limits in the region from CAST (green) SN1987A (light green) are also plotted. Also shown are popular axion model bands, KSVZ (gold, dashed) and DFSZ (blue, dashed).

of $\vec{J}_a = -g_{a\gamma\gamma}\sqrt{\frac{\epsilon_0}{\mu_0}}\vec{B}\frac{\partial a}{\partial t}$. As shown in the appendix, this current density is related to the effective axion charge density $\rho_a = g_{a\gamma\gamma}c\vec{B} \cdot \nabla a$, via a continuity equation $\vec{\nabla} \cdot \vec{J}_a = -\frac{\partial \rho_a}{\partial t}$. Since there are no conductors involved, ρ_a is an effective bound charge and \vec{J}_a an effective displacement current. As shown in the appendix, these values are consistent with the derived value of \vec{E}_a . This displacement current can either be detected directly with a capacitive sensor, or via the induced time-varying magnetic field using an inductive sensor. In ABRACADABRA [26] a loop is placed outside the toroidal magnet to detect the magnetic flux induced by \vec{J}_a (which is located inside the magnet and along the field lines). Our approach is analogous to placing a capacitive detector inside the toroidal magnet in order to detect directly \vec{E}_a or \vec{J}_a . In this analogue we do not strictly need to consider the derivation of the electric and magnetic fields, and achieve equivalent expressions for current and voltage by considering a displacement current flowing across a parallel plate capacitor.

When compared with a typical resonant haloscope we lose the enhancement of the signal by the resonance quality-factor, Q . However, in principal it is possible to combine the signals from several capacitors in the same magnetic field to enhance sensitivity. Typical microwave Q s in axion haloscopes are of order $10^4 - 10^5$, and whilst it is unlikely that combining this many capacitors inside a single magnet bore would be readily achievable, it may be possible to mitigate the loss somewhat through combining capacitors. The optimal strategy for this capacitor combination depends on the method of readout, and various other limitations such as stray capacitance.

When implementing a voltage readout we note that the plate area is unimportant and may thus opt for a number of very small diameter capacitors with large plate separations. In such a case, to avoid issues associated with having very small plate areas with very large plate separations we may instead opt to combine many small capacitors (small plate area and small plate separation) in series to create a “chain” of capacitors, with an effective total plate separation equal to the sum of the plate separations in the chain. This would maintain large effective plate separations, whilst simultaneously allowing for very low plate areas, and thus allowing for many such chains inside the same magnet. To understand how a scheme like this would work, cross capacitance between each element and stray capacitance due to the experimental chamber and grounding would need to be modelled carefully. In contrast, implementing a current readout scheme, large plate areas are required with arbitrary plate separations. In such a scheme it would be optimal to create many small plate separation capacitors with large plate area and then combine the current outputs. Again placement within the magnet bore and the avoidance of stray capacitances or accidental electrical connection of neighbouring capacitors would need to be carefully considered.

Another prospect would be to sense the electric field with an array of long wire dipole antennas aligned along the z -axis and combine the outputs. Oscillating current in the wires would be driven by the oscillating electric field induced by the axion and these currents could be combined. The capacitance and frequency response of such structures are well known, and they are generally broadband with a low frequency cutoff and a high frequency resonance. Such techniques may be suitable in a different mass range to that proposed in this work.

We propose an axion haloscope sensitive to low-mass axions, where a number of capacitors are coupled to a low noise amplifier such as a SQUID or a high impedance amplifier inside a static magnetic field. This measurement is broadband and thus sensitive to axions over a wide range of mass values simultaneously. The bandwidth of the amplifier sets the limit on the detectable mass range. For example, in the case of a SQUID readout the location of the resonance which will be generated by the combination of the capacitor and SQUID input inductor (usually a few MHz) [33] will be the limiting factor. We now project the sensitivities for the experiments discussed above, with the two readout schemes presented and speculate on how to approach the axion model sensitivities.

The spectral density of the RMS axion-induced current from the capacitor can be approximated by

$$\frac{I_{a_{RMS}}}{\sqrt{\pi \times BW}}, \quad (2)$$

where BW is the bandwidth of the axion signal, roughly 10^{-6} times the central frequency. We can combine equa-

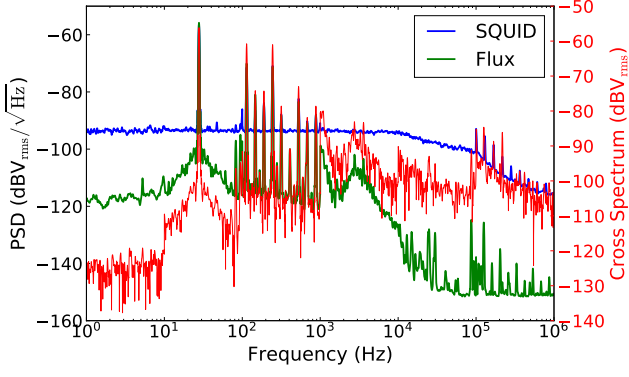


FIG. 3: Voltage noise spectra at the output of the SQUID in the first run of BEAST. The blue (green) trace corresponds to the SQUID (flux) line, whilst the red trace corresponds to the cross-spectrum.

tions (1) and (2) then compare with typical SQUID RMS current spectral density, $0.5 \frac{pA}{\sqrt{Hz}}$, to find the smallest possible $g_{a\gamma\gamma}$ detectable with such a setup as a function of axion mass. For general parameters this is given by,

$$g_{a\gamma\gamma} = \frac{5.2 \times 10^{-20} \sqrt{m}}{AB\sqrt{\rho}}.$$

With m in eV, and everything else in SI units we obtain $g_{a\gamma\gamma}$ in GeV^{-1} . Fig. 2 shows projected limits for 10 cm diameter capacitors embedded in a 14 T magnetic field, coupled to SQUIDS, with arbitrary plate separation and an arbitrary material between the plates, assuming that the dark matter is comprised of axions with an energy density of $0.45 \frac{\text{GeV}}{\text{cm}^3}$.

If we read out capacitor voltage with a high-impedance amplifier, we can follow a very similar process to estimate sensitivity. The effective total voltage noise referred to the input of high-impedance amplifiers depends on a number of factors, but for the purposes of this estimate we use a value of $100 \frac{nV}{\sqrt{Hz}}$ (see appendix for calculations). Defining the peak spectral density of the RMS axion-induced voltage from the capacitor in the same way as for the current, we can arrive at the projected exclusion limits in much the same way. In this case we compare the peak of the axion-induced rms-voltage PSD with the above voltage noise. For general parameters we arrive at,

$$g_{a\gamma\gamma} = \frac{4.4 \times 10^{-10} m^{3/2} \epsilon_r}{Bd\sqrt{\rho}}.$$

With m in eV, and everything else in SI units we obtain $g_{a\gamma\gamma}$ in GeV^{-1} . Fig. 2 also shows projected limits for capacitors (or chains of capacitors) with a net effective plate separation of 0.4 m, with vacuum between the plates, and assuming again that the dark matter is comprised of axions with an energy density of $0.45 \frac{\text{GeV}}{\text{cm}^3}$.

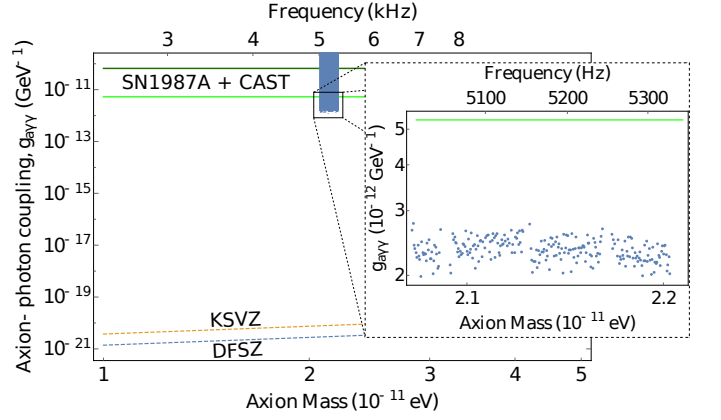


FIG. 4: Exclusion limits calculated from a single capacitor coupled to a SQUID. Previous best limits in the region from CAST (green) SN1987A (light green) are also plotted. Also shown are the axion model bands, KSVZ (gold, dashed) and DFSZ (blue, dashed). The inset shows the actual limit as a function of mass, including narrow regions where limits could not be placed due to large noise sources.

We note that this detection method, due to its broad-band nature, is preferable to traditional haloscopes in searching for transient enhancements in the flux of axions through the earth, such as those expected in the case of axion miniclusters [34], or axion dark matter streaming [35]. A traditional haloscope might miss such an event, due to being tuned away from the mass of the axion, whereas with this detector, if the axion mass falls within the bandwidth of the search we would be sensitive to these short-lived, but enormous boosts in sensitivity. Our first BEAST experiment consists of a simple parallel plate capacitor coupled to a SQUID amplifier. In this experiment a 7.5×7 cm rectangular capacitor was embedded in a 7 T field at 4 K for 8 days of observation time. The capacitor was coupled to a SQUID with a -3 dB bandwidth of 2.1 MHz and a transimpedance of 1.2 M Ω . Fig. 3 shows spectra obtained up to 1 MHz with the associated spurious signals in this region. However, it is possible to discriminate against these spurious signals with the flux line, which is susceptible to spurious RF signals in the lab. These spectra do not have the requisite spectral resolution to resolve axion signals with an effective linewidth of $10^{-6} \times \omega_a$, but serve to demonstrate the expected output spectra of such an experiment and highlight the issue of spurious noise sources.

A higher-resolution search was conducted around 5 kHz, with the minimal spectral resolution of 4.5 mHz (increasing at higher frequencies), thus providing the requisite spectral resolution to detect ALP signals. All sharp peaks greater than ~ 4.4 standard deviations from the mean originating from the SQUID were able to be excluded, due to a similar signal appearing in the flux line,

as shown in fig. 3. Using this data, we may place the 95 % confidence exclusion limits on axion-photon coupling shown in fig. 4. The average limit is $g_{a\gamma\gamma} > \sim 2.35 \times 10^{-12}$, with some variation as a function of mass. This experiment serves as a proof of concept, and can be readily extended to wider mass ranges.

In conjunction with the planned ORGAN experiment [25], we are developing the BEAST experiment for low-mass searches to run in parallel, utilizing the extra space in the ORGAN 14 T magnet bore. Technical limitations with availability of equipment, data acquisition and processing prevented a wider search from being feasible within the time scale of this first experiment, however in the future a dedicated system will be built and FPGA-based solutions to data acquisition issues will be implemented. Note, that if a direct voltage readout was employed via a high-impedance amplifier, we would not necessarily need to conduct the experiment cryogenically, as the noise floors of these devices are exceptionally low even at room temperature. Rare-earth magnets are capable of achieving magnetic fields on the order of a Tesla and, unlike superconducting solenoids, require no cryogenic environment to operate. Although these fields are considerably lower than those achievable with superconducting solenoids, an experiment could be conducted on a bench-top, without the need of a dedicated cryogenic cooler or magnet, and could operate continuously for very long times.

This work was funded by Australian Research Council (ARC) grant No. CE170100009, the Australian Government's Research Training Program, and the Bruce and Betty Green Foundation.

* ben.mcallister@uwa.edu.au

† michael.tobar@uwa.edu.au

- [1] V. C. Rubin, W. K. Ford, Jr., and N. Thonnard, *Astrophys. J.* **238**, 471 (1980).
- [2] M. Markevitch, A. H. Gonzalez, D. Clowe, A. Vikhlinin, W. Forman, C. Jones, S. Murray, and W. Tucker, *Astrophys. J.* **606**, 819 (2004).
- [3] R. Barkana, *Nature*, **555**, 71 (2018).
- [4] J. D. Bowman, A. E. E. Rogers, R. A. Monsalve, T. J. Mozdzen, and N. Mahesh, *Nature*, **555**, 67 (2018).
- [5] E. Aprile, J. Aalbers, F. Agostini, M. Alfonsi, F. D. Amaro, M. Anthony, F. Arneodo, P. Barrow, L. Baudis, B. Bauermeister, M. L. Benabderrahmane, T. Berger, P. A. Breur, A. Brown, A. Brown, E. Brown, S. Bruenner, G. Bruno, R. Budnik, L. Bütikofer, J. Calvén, J. M. R. Cardoso, M. Cervantes, D. Cichon, D. Coderre, A. P. Colijn, J. Conrad, J. P. Cussonneau, M. P. Decowski, P. de Perio, P. Di Gangi, A. Di Giovanni, S. Diglio, G. Eurin, J. Fei, A. D. Ferella, A. Fieguth, W. Fulgione, A. Gallo Rosso, M. Galloway, F. Gao, M. Garbini, R. Gardner, C. Geis, L. W. Goetzke, L. Grandi, Z. Greene, C. Grignon, C. Hasterok, E. Hogenbirk, J. Howlett, R. Itay, B. Kaminsky, S. Kazama, G. Kessler, A. Kish, H. Landsman, R. F. Lang, D. Lellouch, L. Levinson, Q. Lin, S. Lindemann, M. Lindner, F. Lombardi, J. A. M. Lopes, A. Manfredini, I. Maris, T. Marrodán Undagoitia, J. Masbou, F. V. Massoli, D. Masson, D. Mayani, M. Messina, K. Micheneau, A. Molinaro, K. Mora, M. Murra, J. Naganoma, K. Ni, U. Oberlack, P. Pakarha, B. Pelssers, R. Persiani, F. Piastra, J. Pienaar, V. Pizzella, M.-C. Piro, G. Plante, N. Priel, L. Rauch, S. Reichard, C. Reuter, B. Riedel, A. Rizzo, S. Rosendahl, N. Rupp, R. Saldanha, J. M. F. dos Santos, G. Sartorelli, M. Scheibelhut, S. Schindler, J. Schreiner, M. Schumann, L. Scotto Lavina, M. Selvi, P. Shagin, E. Shockley, M. Silva, H. Simgen, M. v. Sivers, A. Stein, S. Thapa, D. Thers, A. Tiseni, G. Trincherro, C. Tunnell, M. Vargas, N. Upole, H. Wang, Z. Wang, Y. Wei, C. Weinheimer, J. Wulf, J. Ye, Y. Zhang, and T. Zhu (XENON Collaboration), *Phys. Rev. Lett.* **119**, 181301 (2017).
- [6] R. D. Peccei and H. R. Quinn, *Phys. Rev. Lett.* **38**, 1440 (1977).
- [7] F. Wilczek, *Phys. Rev. Lett.* **40**, 279 (1978).
- [8] J. Jaeckel and A. Ringwald, *Annual Review of Nuclear and Particle Science* **60**, 405 (2010).
- [9] J. Ipser and P. Sikivie, *Phys. Rev. Lett.* **50**, 925 (1983).
- [10] P. Sikivie, *Phys. Rev. Lett.* **51**, 1415 (1983).
- [11] P. Sikivie, *Phys. Rev. D* **32**, 2988 (1985).
- [12] J. E. Kim, *Phys. Rev. Lett.* **43**, 103 (1979).
- [13] J. E. Kim and G. Carosi, *Rev. Mod. Phys.* **82**, 557 (2010).
- [14] M. Dine, W. Fischler, and M. Srednicki, *Physics Letters B* **104**, 199 (1981).
- [15] M. Shifman, A. Vainshtein, and V. Zakharov, *Nuclear Physics B* **166**, 493 (1980).
- [16] M. Dine and W. Fischler, *Physics Letters B* **120**, 137 (1983).
- [17] L. Abbott and P. Sikivie, *Physics Letters B* **120**, 133 (1983).
- [18] J. Preskill, M. B. Wise, and F. Wilczek, *Physics Letters B* **120**, 127 (1983).
- [19] G. Ballesteros, J. Redondo, A. Ringwald, and C. Tamarit, *Phys. Rev. Lett.* **118**, 071802 (2017).
- [20] S. J. Asztalos, G. Carosi, C. Hagmann, D. Kinion, K. van Bibber, M. Hotz, L. J. Rosenberg, G. Rybka, J. Hoskins, J. Hwang, P. Sikivie, D. B. Tanner, R. Bradley, and J. Clarke, *Phys. Rev. Lett.* **104**, 041301 (2010).
- [21] J. Hoskins, J. Hwang, C. Martin, P. Sikivie, N. S. Sullivan, D. B. Tanner, M. Hotz, L. J. Rosenberg, G. Rybka, A. Wagner, S. J. Asztalos, G. Carosi, C. Hagmann, D. Kinion, K. van Bibber, R. Bradley, and J. Clarke, *Phys. Rev. D* **84**, 121302 (2011).
- [22] A. Caldwell, G. Dvali, B. Majorovits, A. Millar, G. Raffelt, J. Redondo, O. Reimann, F. Simon, and F. Steffen (MADMAX Working Group), *Phys. Rev. Lett.* **118**, 091801 (2017).
- [23] B. M. Brubaker, L. Zhong, Y. V. Gurevich, S. B. Cahn, S. K. Lamoreaux, M. Simanovskaia, J. R. Root, S. M. Lewis, S. Al Kenany, K. M. Backes, I. Urdinaran, N. M. Rapidis, T. M. Shokair, K. A. van Bibber, D. A. Palken, M. Malnou, W. F. Kindel, M. A. Anil, K. W. Lehnert, and G. Carosi, *Phys. Rev. Lett.* **118**, 061302 (2017).
- [24] W. Chung, *Proceedings, 15th Hellenic School and Workshops on Elementary Particle Physics and Gravity (CORFU2015): Corfu, Greece, September 1-25, 2015*, *PoS CORFU2015*, 047 (2016).
- [25] B. T. McAllister, G. Flower, E. N. Ivanov, M. Goryachev,

- J. Bourhill, and M. E. Tobar, Physics of the Dark Universe **18**, 67 (2017).
- [26] Y. Kahn, B. R. Safdi, and J. Thaler, Phys. Rev. Lett. **117**, 141801 (2016),.
- [27] B. T. McAllister, G. Flower, L. E. Tobar, and M. E. Tobar, Phys. Rev. Applied **9**, 014028 (2018).
- [28] P. Sikivie, N. Sullivan, and D. B. Tanner, Phys. Rev. Lett. **112**, 131301 (2014).
- [29] B. T. McAllister, S. R. Parker, and M. E. Tobar, Phys. Rev. **D94**, 042001 (2016),.
- [30] O. Reimann, “A novel microwave axion-detector,” (2016), “Detectors And Instrumentation Workshop”, Max-Planck-Institut für Physik.
- [31] B. T. McAllister, S. R. Parker, and M. E. Tobar, Phys. Rev. Lett. **116**, 161804 (2016), [Erratum: Phys. Rev. Lett. **117**, no.15, 159901 (2016)],.
- [32] E. J. Daw, *A search for halo axions*, Ph.D. thesis, MIT (1998).
- [33] M. Goryachev, E. N. Ivanov, F. van Kann, S. Galliou, and M. E. Tobar, Applied Physics Letters **105**, 153505 (2014), <https://doi.org/10.1063/1.4898813>.
- [34] M. Fairbairn, D. J. E. Marsh, J. Quevillon and S. Rozier, Phys. Rev. D **97**, no. 8, 083502 (2018) doi:10.1103/PhysRevD.97.083502 [arXiv:1707.03310 [astro-ph.CO]].
- [35] K. Zioutas *et al.*, arXiv:1703.01436 [physics.ins-det].
- [36] *HFC 50 D / E Dual Cryogenic Ultra Low Noise RF-Amplifier*, Stahl Electronics (2016), version 2.38.
- [37] Benjamin M. Brubaker. *First results from the HAYSTAC axion search*. PhD thesis, Yale U., 2017.

APPENDIX

Details of Current and Voltage Derivation

We begin with the electric and magnetic fields induced by axions inside a uniform z-direction magnetic field.

$$\begin{aligned}\vec{E}_a &= E_a \hat{z} = \frac{1}{\epsilon_r} g_{a\gamma\gamma} c B_0 a \hat{z} \\ \vec{B}_a &= \mu_r \frac{1}{2} \frac{g_{a\gamma\gamma}}{c} r B_0 \frac{\partial a}{\partial t} \hat{\phi}.\end{aligned}$$

Here r is the distance from the centre of the solenoid, and \hat{z} and $\hat{\phi}$ are the z-direction and ϕ -direction unit vectors in the cylindrical co-ordinate system of the solenoid.

In this section we consider the signal from a parallel plate capacitor embedded in the magnetic field, such that the vector area of the plates are aligned with the induced electric field. The capacitance of a parallel plate capacitor with plate area A and separation d is given by $C = \frac{\epsilon_0 \epsilon_r A}{d}$. The voltage across the plates as a result of the axion induced electric field, \vec{E}_a is given by

$$\begin{aligned}V &= \int_0^d E_a dz \\ &= \frac{1}{\epsilon_r} g_{a\gamma\gamma} c B_0 a d,\end{aligned}$$

where $a = a_0 \cos(\omega_a t)$. Now

$$\begin{aligned}I &= C \frac{dV}{dt} \\ &= -C \frac{\omega_a}{\epsilon_r} g_{a\gamma\gamma} c B_0 d a_0 \sin(\omega_a t) \\ &= -A \epsilon_0 \omega_a g_{a\gamma\gamma} c B_0 a_0 \sin(\omega_a t).\end{aligned}$$

Where we have used $C = \frac{\epsilon_0 \epsilon_r A}{d}$. It can be shown that $a_0 = \sqrt{\frac{2\rho_a}{c} \frac{\hbar}{m_a}}$ [32], so

$$\begin{aligned}I_a(t) &= -g_{a\gamma\gamma} \epsilon_0 A B_0 \sqrt{2\rho_a c^5} \sin(\omega_a t) \\ V_a(t) &= \frac{1}{\epsilon_r} g_{a\gamma\gamma} B_0 \sqrt{2\rho_a c} \frac{\hbar}{m_a} d \cos(\omega_a t),\end{aligned}$$

or, for the RMS values

$$\begin{aligned}I_{a_{RMS}} &= -g_{a\gamma\gamma} \epsilon_0 A B_0 \sqrt{\rho_a c^5} \\ V_{a_{RMS}} &= \frac{1}{\epsilon_r} g_{a\gamma\gamma} B_0 \sqrt{\rho_a c^5} \frac{1}{\omega_a} d.\end{aligned}$$

Details of Input Voltage Noise of High-impedance amplifier

In considering the effective voltage noise of the amplifier, referred to the input (δu_{eff}) we must consider contributions as a result of the input voltage noise (δu_V), the input current noise (δu_I), and the thermal input noise (δu_{Th}). This can be presented as,

$$\delta u_{eff} = \sqrt{\delta u_V^2 + \delta u_I^2 + \delta u_{Th}^2}.$$

We will now discuss each of these quantities. δu_I and δu_{Th} must be found via,

$$\begin{aligned}\delta u_I &= \delta i_{amp} \times |Z|, \\ \delta u_{Th} &= \delta i_{Th} \times |Z|.\end{aligned}$$

Here δi_{amp} is in the intrinsic amplifier current noise and δi_{Th} is the thermally induced current noise given by

$$\delta i_{Th} = \sqrt{\frac{k_B T_0}{R_{amp}}},$$

where k_B is the Boltzmann constant, T is the physical temperature, and R_{amp} is the amplifier input resistance, and finally Z is the complex impedance of the amplifier and capacitor system given by

$$Z = \frac{R_{amp}}{1 + i2\pi f C R_{amp}},$$

where C takes into account the capacitance of the detector C_{det} and the input capacitance of the amplifier C_{amp} such that,

$$C = \frac{C_{det} C_{amp}}{C_{det} + C_{amp}}.$$

The final quantity, δu_V arises from the intrinsic amplifier input voltage noise δu_{amp} according to

$$\delta u_V = \delta u_{amp} \times \left| \frac{Z_{amp}}{Z_{amp} + Z_{det}} \right|.$$

Where Z_{amp} and Z_{det} are the amplifier and detector impedances given by

$$\begin{aligned}Z_{amp} &= \frac{R_{amp}}{1 + i2\pi f C_{amp} R_{amp}}, \\ Z_{det} &= \frac{1}{2\pi f C_{det}}.\end{aligned}$$

Taking the values for these equations from a suitable datasheet [36] and the detector parameters proposed in the main text, we arrive at a value for δu_{eff} which is roughly constant as a function of frequency, at $\delta u_{eff} \approx 1 \times 10^{-7} \frac{V}{\sqrt{Hz}}$ from 1 kHz to 1 MHz. This will be heavily dependent on the specific parameters of the amplifier and detector, but for the purposes of these sensitivity estimates this is the value we employ.

Details of Electric and Magnetic Field Derivation

We begin with the following Maxwell's equations generalized for media, in the presence of external sources including an axion coupled to photons, adapted from [30],

$$\epsilon_r \vec{\nabla} \cdot (\vec{E}_0 + \vec{E}_a) = \frac{\rho}{\epsilon_0} + g_{a\gamma\gamma} c (\vec{B}_0 + \vec{B}_a) \cdot \nabla a, \quad (3)$$

$$\begin{aligned}\frac{1}{\mu_r} \vec{\nabla} \times (\vec{B}_0 + \vec{B}_a) - \frac{1}{c^2} \epsilon_r \frac{\partial (\vec{E}_0 + \vec{E}_a)}{\partial t} = \\ \mu_0 \vec{J} - \frac{g_{a\gamma\gamma}}{c} \left((\vec{B}_0 + \vec{B}_a) \frac{\partial a}{\partial t} + \nabla a \times (\vec{E}_0 + \vec{E}_a) \right),\end{aligned} \quad (4)$$

$$\vec{\nabla} \cdot (\vec{B}_0 + \vec{B}_a) = 0, \quad (5)$$

$$\vec{\nabla} \times (\vec{E}_0 + \vec{E}_a) = -\frac{\partial (\vec{B}_0 + \vec{B}_a)}{\partial t}. \quad (6)$$

Here, the fields \vec{E}_0 and \vec{B}_0 are the fields applied in the experiment, \vec{E}_a and \vec{B}_a are the fields induced by axion-photon conversion, μ_r and ϵ_r are the relative permeability and permittivity of the medium in question, $g_{a\gamma\gamma}$ is the axion-photon coupling constant, ρ is the charge density, \vec{J} is the current density, a is the axion scalar field and c is the speed of light.

In haloscopes

We make a number of assumptions that apply in the context of the axion dark matter haloscope, where a static magnetic field is supplied by a solenoid, and we are in cylindrical coordinates (r, ϕ, z) :

$$\begin{aligned}a &= a_0 \cos(\omega_a t + \vec{k}_a \cdot \vec{r}), \\ \vec{B}_0 &= B_0 \hat{z}, \\ \vec{E}_0 &= 0, \\ \vec{E}_a &\sim \mathcal{O}(g_{a\gamma\gamma}), \\ \vec{B}_a &\sim \mathcal{O}(g_{a\gamma\gamma}).\end{aligned} \quad (7)$$

Here ω_a is the Compton frequency of the axion, and \vec{k}_a the wave vector, which we take to be small in the following calculations. Further, since in a typical haloscope with a large applied magnetic field

$$\vec{B}_0 \gg \vec{B}_a,$$

we initially take the (common [37]) approximation that

$$\vec{B}_0 + \vec{B}_a \approx \vec{B}_0. \quad (8)$$

We will re-visit this final assumption later, in the context of demonstrating self-consistency of the solutions we obtain. We further assume that we are in free space ($\epsilon_r = \mu_r = 1$, $\vec{J} = \rho = 0$). Under the above assumptions,

we can reduce the Maxwell's equations to first order in $g_{a\gamma\gamma}$, dropping terms of order $g_{a\gamma\gamma}^2$ or higher.

$$\vec{\nabla} \cdot \vec{E}_a = g_{a\gamma\gamma} c \vec{B}_0 \cdot \nabla a, \quad (9)$$

$$\vec{\nabla} \times \vec{B}_0 - \frac{1}{c^2} \frac{\partial \vec{E}_a}{\partial t} = -\frac{g_{a\gamma\gamma}}{c} \left(\vec{B}_0 \frac{\partial a}{\partial t} \right), \quad (10)$$

$$\vec{\nabla} \cdot \vec{B}_0 = 0, \quad (11)$$

$$\vec{\nabla} \times \vec{E}_a = -\frac{\partial \vec{B}_0}{\partial t}. \quad (12)$$

Induced electric and magnetic fields

We now focus on (10) and, since $\vec{B}_0 = B_0 \hat{z}$, $\nabla \times \vec{B}_0 = 0$, which (integrating over time) leads us to

$$\vec{E}_a = g_{a\gamma\gamma} c B_0 a \hat{z}. \quad (13)$$

It is trivial to show that this field satisfies (9) - (12). Furthermore, assuming $\vec{B}_a = B_a \hat{\phi}$ the Ampere-Maxwell law gives us

$$\oint_C \vec{B}_a \cdot d\vec{l} = \frac{1}{c^2} \frac{\partial}{\partial t} \int \int_S \vec{E}_a \cdot d\vec{S}. \quad (14)$$

We take S to be a circular surface inside the solenoid with radius r , and C to be the boundary of this circular surface. Substituting (13) into (14) and integrating we obtain

$$B_a \times 2\pi r = \frac{g_{a\gamma\gamma}}{c} B_0 \frac{\partial a}{\partial t} \times \pi r^2,$$

and finally

$$\vec{B}_a = \frac{g_{a\gamma\gamma}}{2c} r B_0 \frac{\partial a}{\partial t} \hat{\phi}. \quad (15)$$

This method is consistent with typical calculations undertaken to derive magnetic fields in the presence of uniform electric fields (such as those between capacitor plates).

Continuity equation approach

From the axion source terms in the modified Maxwell's equations (9 and 10) we may define the following;

$$\rho_a = g_{a\gamma\gamma} \sqrt{\frac{\epsilon_0}{\mu_0}} \vec{B}_0 \cdot \nabla a, \quad (16)$$

$$\vec{J}_a = -g_{a\gamma\gamma} \sqrt{\frac{\epsilon_0}{\mu_0}} \left(\vec{B}_0 \frac{\partial a}{\partial t} \right). \quad (17)$$

Since there are no free charges or conducting electrons, we interpret ρ_a as a vacuum bound charge and \vec{J}_a as

a displacement current. It is straightforward to show they satisfy the continuity equation. Taking the time derivative of eqn. (16) we obtain;

$$\frac{\partial \rho_a}{\partial t} = g_{a\gamma\gamma} \sqrt{\frac{\epsilon_0}{\mu_0}} \vec{B}_0 \cdot \nabla \frac{\partial a}{\partial t}. \quad (18)$$

Then by taking the divergence of eqn. (17) we obtain

$$\nabla \cdot \vec{J}_a = -g_{a\gamma\gamma} \sqrt{\frac{\epsilon_0}{\mu_0}} \nabla \cdot \left(\vec{B}_0 \frac{\partial a}{\partial t} \right). \quad (19)$$

Using standard vector calculus identities and the fact that $\nabla \cdot \vec{B}_0 = 0$ we obtain;

$$\nabla \cdot \vec{J}_a = -g_{a\gamma\gamma} \sqrt{\frac{\epsilon_0}{\mu_0}} \vec{B}_0 \cdot \nabla \frac{\partial a}{\partial t}. \quad (20)$$

Combining eqns. (18) and (20) we prove the continuity equation;

$$\nabla \cdot \vec{J}_a = -\frac{\partial \rho_a}{\partial t}. \quad (21)$$

It is then easy to show that the effective current density, \vec{J}_a , due to the displacement of effective bound charge, ρ_a , is related to E_a by;

$$\vec{J}_a = -\epsilon_0 \frac{\partial \vec{E}_a}{\partial t}. \quad (22)$$

Thus by equating eqns (17) and (22) the electric field due to conversion of axions, oscillating at the Compton frequency may be verified to be consistent with eqn. (13).

Further self-consistency checking

It is important to note that in deriving the electric field (13), we make approximation (8), and subsequently drop \vec{B}_a terms from the modified Maxwell's equations (9) - (12). Indeed, under approximation (8) the equations are all satisfied by electric and magnetic fields (13) and (15). Hence, these solutions are valid in cases where approximation (8) holds. This is typically where the derivation would cease, but we can go a step further and verify that upon inserting (13) and (15) back into, for example, equations (3) - (6) we can still achieve a self-consistent solution. We will begin with equations (3) - (6) subject to the assumptions outlined in (7) (slightly re-arranged), but not assumption (8). We have

$$\vec{\nabla} \times (\vec{B}_0 + \vec{B}_a) = \frac{1}{c^2} \frac{\partial \vec{E}_a}{\partial t} - \frac{g_{a\gamma\gamma}}{c} \left(\vec{B}_0 \frac{\partial a}{\partial t} \right), \quad (23)$$

$$\vec{\nabla} \times \vec{E}_a = -\frac{\partial (\vec{B}_0 + \vec{B}_a)}{\partial t}. \quad (24)$$

Note that \vec{B}_a is still absent on the right hand side of (23) as the resulting term would be of order $g_{a\gamma\gamma}^2$ when expanded. Taking the curl of both sides of (24) yields

$$\nabla \left(\nabla \cdot \vec{E}_a \right) - \nabla^2 \vec{E}_a = - \frac{\partial \left(\nabla \times (\vec{B}_0 + \vec{B}_a) \right)}{\partial t}. \quad (25)$$

Substituting the reduced (3) and (23) into (25) yields

$$\begin{aligned} \nabla \left(g_{a\gamma\gamma} c (\vec{B}_0 + \vec{B}_a) \cdot \nabla a \right) - \nabla^2 \vec{E}_a = \\ - \frac{\partial \left(\frac{1}{c^2} \frac{\partial \vec{E}_a}{\partial t} - \frac{g_{a\gamma\gamma}}{c} \left(\vec{B}_0 \frac{\partial a}{\partial t} \right) \right)}{\partial t}. \end{aligned}$$

Now, assuming that since the axion wave vector is small all spatial derivatives of a , \vec{E}_a , and \vec{B}_a are small and can be neglected compared to terms without spatial deriva-

tives, we are left with

$$0 = - \frac{1}{c^2} \frac{\partial^2 \vec{E}_a}{\partial t^2} + \frac{g_{a\gamma\gamma}}{c} \vec{B}_0 \frac{\partial^2 a}{\partial t^2},$$

which it is trivial to show is satisfied on substitution of (13). The solutions (13) and (15) for electric and magnetic fields induced by axions are approximately valid, which is supported by the fact that the electric and magnetic fields take on similar forms to the electric and magnetic fields inside a capacitor with a uniform displacement current density flowing between the plates. This makes sense, given that an effective displacement current density is a popular model for the axion-induced electromagnetic effects.

We further note that the axion-induced magnetic field derived here (15) agrees with the magnetic field in a right cylindrical solenoid as derived by Sikivie in his LC circuit paper [28], and the electric and magnetic fields must be consistent with one another via the Ampere-Maxwell law.